Air Traffic Radar Interference Event in the Galileo E6 Band: Detection, Analysis and Mitigation

Javier Arribas, *Centre Tecnològic de Telecomunicacions de Catalunya (CTTC/CERCA)*, Spain.
Antonio Ramos de Torres, *Signal Theory and Communications Department, Polytechnic University of Catalonia*, Spain.
Carles Fernández–Prades, *Centre Tecnològic de Telecomunicacions de Catalunya (CTTC/CERCA)*, Spain.
Jordi Vilà-Valls, *Centre Tecnològic de Telecomunicacions de Catalunya (CTTC/CERCA)*, Spain.
Pau Closas, *Electrical and Computer Engineering Dept., Northeastern University*, Boston, MA, USA.

BIOGRAPHIES

Dr. Javier Arribas holds the position of Senior Researcher at the Statistical Inference for Communications and Positioning (SI) Department at CTTC. He received the MSc degree in Telecommunication Engineering from La Salle University in 2004, and the PhD from UPC in 2012. His primary areas of interest include statistical signal processing, GNSS synchronization, detection and estimation theory, software defined receivers, FPGA prototyping and the design of RF front-ends. He is the recipient of the 2015 EURASIP Best PhD Thesis Award.

Mr. Antonio Ramos de Torres is a Ph.D Candidate in the Signal Theory and Communications Department of the Universitat Politècnica de Catalunya (UPC). He received the MSc degree in Telecommunication Engineering from UPC in 2013. His primary areas of interest include statistical signal processing with application in spectroscopy analysis techniques and GNSS software defined receivers.

Dr. Jordi Vilà-Valls is a Researcher at the SI Department at Centre CTTC, Barcelona, Spain. He received the PhD degree in Electrical Engineering from Grenoble INP (INPG), France, in 2010. His primary areas of interest include statistical signal processing, estimation and detection theory, robustness and adaptive methods; with applications to GNSS, positioning/tracking systems, wireless communications and aerospace science.

Dr. Carles Fernández–Prades holds the position of Senior Researcher and serves as Head of the SI Dept. at CTTC. He received a PhD degree in Electrical Engineering from Universitat Politècnica de Catalunya (UPC) in 2006, Barcelona, Spain. His primary areas of interest include statistical and multi-sensor signal processing, estimation and detection theory, and Bayesian filtering, with application in communication systems, GNSS and software-defined radio technology.

Dr. Pau Closas is Assistant Professor at Northeastern University, Boston, MA. He received the MSc and PhD degrees in Electrical Engineering from UPC in 2003 and 2009, respectively. He also holds a MSc degree in Advanced Mathematics and Mathematical Engineering from UPC since 2014. His primary areas of interest include statistical signal processing, robust stochastic filtering, and game theory, with applications to positioning systems and wireless communications. He is the recipient of the 2014 EURASIP Best PhD Thesis Award, the 9th Duran Farell Award, and the 2016 ION Early Achievements Award.

ABSTRACT

In this work, the authors report a serious threat to the Galileo E6 users caused by an in-band L-band Air Traffic Control (ATC) radar pulsed interference, which is currently *authorized* by the International Telecommunications Union radio regulations in Europe. This paper documents the complete sequence of facts in a real environment, from the interference detection, time/frequency analysis, source identification and location to the mitigation of its effects by implementing a real-time pulse blanking algorithm in an open source, software defined GNSS receiver. The vulnerability of general purpose front-ends to strong out-of-band interferences due to lack of selectivity and component non-linearities was also evidenced, which is specially concerning for Software Defined Radio (SDR) receiver users. In order to assess the interference protection options of a receiver, three input filter blocks have been implemented and integrated into the open source GNSS-SDR receiver. These signal processing blocks aim to mitigate two common types of interferences: continuous wave FM modulated and short-time pulsed ones. Two blocks deal with the CW interferences, implementing an adaptive Notch filter interference canceler. The first implementation performs a very effective mitigation of CW interferences even in cases of very fast instantaneous frequency variations. The second implementation requires less computational resources and is valid only when the instantaneous frequency changes relatively slowly. The third block is a Pulse Blanking filter that mitigates pulsed interferences. Both algorithm implementations were tested with real GNSS signals. In case of notch filters, the GNSS signal was contaminated with simulated Continuous Wave FM interferences and, in the case of the pulse blanking algorithm, the performance measurements were obtained using real ATC radar interference captures.

1. INTRODUCTION

The vulnerability of Global Navigation Satellite Systems (GNSS) systems to Radio Frequency Interferences (RFI), either intentional or unintentional, is a fact widely studied in recent times [1]. The performance degradation and even the denial-of-service situations are especially important for safety-critical operations, such as aeronautical high-accuracy positioning and navigation or for distributed timing services. One of the most powerful unintentional interference source comes from the Radionavigation aids. In particular, the civil Air Traffic Control (ATC) primary and secondary surveillance radars operated in the L-Band (1250 MHz 1350 MHz) are very close to the Galileo E5 (1189 MHz) and GPS L5 (1207.140 MHz) bands, and due to its high power pulsed transmissions, which can reach values of tens of Kilowatts, are disrupting the GNSS service, as reported in [2], [3] [4] [5] among others. Fortunately, the ATC interference in Galileo E5 and GPS L5 represents an out-band interference that can be mitigated using sharper bandpass filters in the receiver front-end, among other methods [4].

In February 2017, the European Commission and the European GNSS Agency (GSA) confirmed that the first generation of Galileo satellites would already provide users with high accuracy and authentication services on the Galileo E6 band (1260 MHz to 1300 MHz), this is referred to as the Galileo Commercial Service (CS) [6]. The ATC interference scenario for the Galileo E6 is particularly problematic due to the following facts:

- The Galileo E6 band is completely overlapped with the ATC L-Band, which produces a strong pulsed in-band interference that cannot be mitigated using an antenna filter. This is especially problematic if the receiver uses a multi-band antenna (such as E1/L1 + E5/L5 + E6).

- The current International Telecommunication Union (ITU) regulations [7] and the European radiofrequency spectrum regulation gives priority to the Radionavigation aids, and relegates the GNSS service (referred to as "Radionavigation-satellite" in the official regulation documentation) as a secondary user of the spectrum, as reported in the European table of frequency allocations and applications in the frequency range of 8.3 kHz to 3000 GHz (ECA TABLE [8]).

- The existing legacy ATC L-Band radars, which should be progressively migrated to the S-Band, are still in their medium lifespan.

The confluence of these factors guarantees the persistence of the interference for several years in the future. The authors of this paper detected such situation in Spain, in the Barcelona metropolitan area during their daily research activity.

This paper reports the complete sequence of facts in a real environment, from the interference detection, time/frequency analysis, source identification and location to the mitigation of its effects by implementing a real-time pulse blanking algorithm

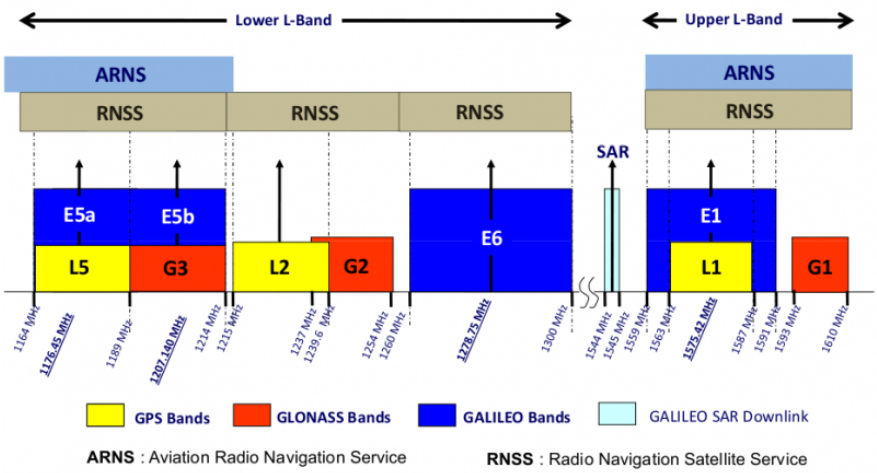

Fig. 1. GNSS bands frequency allocation (source: http://www.navipedia.net/).

[9] in an open source, software defined GNSS receiver [10]. The work also includes a detailed survey of the most popular interference mitigation techniques for single antenna receivers.

The paper is organized as follows: Section 2 introduces the ATC interference event and the facts detected in the Barcelona metropolitan area as reported by the authors to the national radio frequency management authorities. Section 3 briefly introduces the single-antenna interference signal models for both Continuous Wave Interferences (CWI) and pulsed interferences. Section 4 introduces an interference detection algorithm. In Section 5, it is presented the proposed algorithm for CWI interferences mitigation, implementation details and performance results obtained using real GNSS signals contaminated with simulated interferences. In Section 6, it is presented the implemented algorithm for pulsed interferences mitigation and the performance results when it is applied to the real-world interference signals as recorded in the research facilities. Finally, Section 7 provides information of how to configure and use the new interference mitigation blocks implemented in GNSS-SDR, and Section 8 concludes the paper.

2. ATC RADAR INTERFERENCE EVENT

On February 2016, the GESTALT® (GNSS SignAL Testbed) lab facility (see [11] for a detailed description of the GNSS hardware and software set) located at the Centre Tecnològic de Telecomunicacions de Catalunya (CTTC) headquarters in Castelldefels (Barcelona, Spain) was used to capture and analyze the new Galileo E6 signals transmitted in the RF band from 1260 MHz to 1300 MHz, as shown in the GNSS frequency allocation diagram of Fig. 1.

For the experiment, we used a geodetic-grade GNSS active antenna NavXperience 3G+C (E1, E5a, E5b, E5a+b, E6 band support) located in a platform at the roof of CTTC headquarters, as shown in Fig. 2. The RF front-end was a USRP X310 equipped with a SBX daughterboard, tuned at 1278.75 MHz with a sampling rate of 20 MSps.

The time analysis revealed a concerning situation: the signal was severely interfered by an unknown pulsed interference, as shown in Fig. 3. The pulse power was orders of magnitude stronger than the thermal noise floor as shown in Fig. 4. A zoom plot, available on Fig. 5, shows that each pulse had a chirp-shaped waveform.

In order to measure the interference power and its frequency signature, a spectrum analyzer was used to explore the complete GNSS band and its neighborhood. Figure 6 shows an exploration from 1 GHz to 1.6 GHz. It revealed two predominant peaks located at 1.2655 GHz, with -62.78 dBm, and 1.321 GHz with -68.26 dBm. Both time analysis and frequency analysis results indicated that the most likely source of the interference was an ATC radar. The interference signature matched the L-band ATC primary radar spectral characteristics described in [2]. The last clue to find the interference source was obtained just doing quick search on the horizon. Figure 8 shows a picture taken from the GNSS antenna location revealing the Barcelona ATC radar in the receiver line of sight. It is important to highlight that this situation was not a single isolated event, but sustained in time due to the ATC radar continuous operation.

Fig. 2. GESTALT antenna array facility.

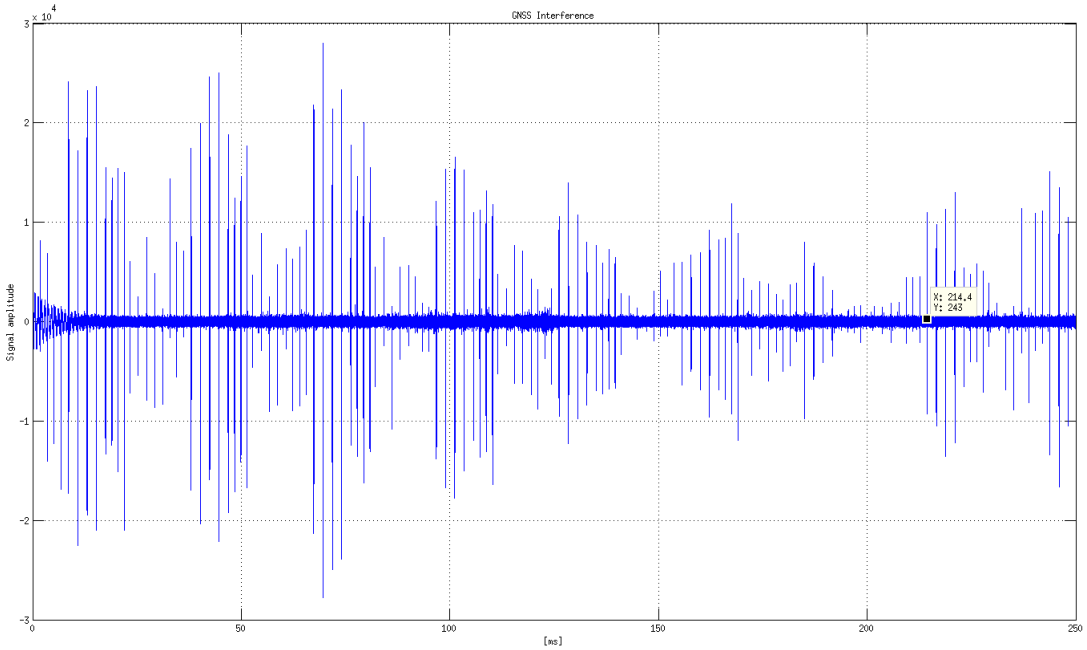

Fig. 3. Galileo E6 signal with the presence of unknown pulsed interference.

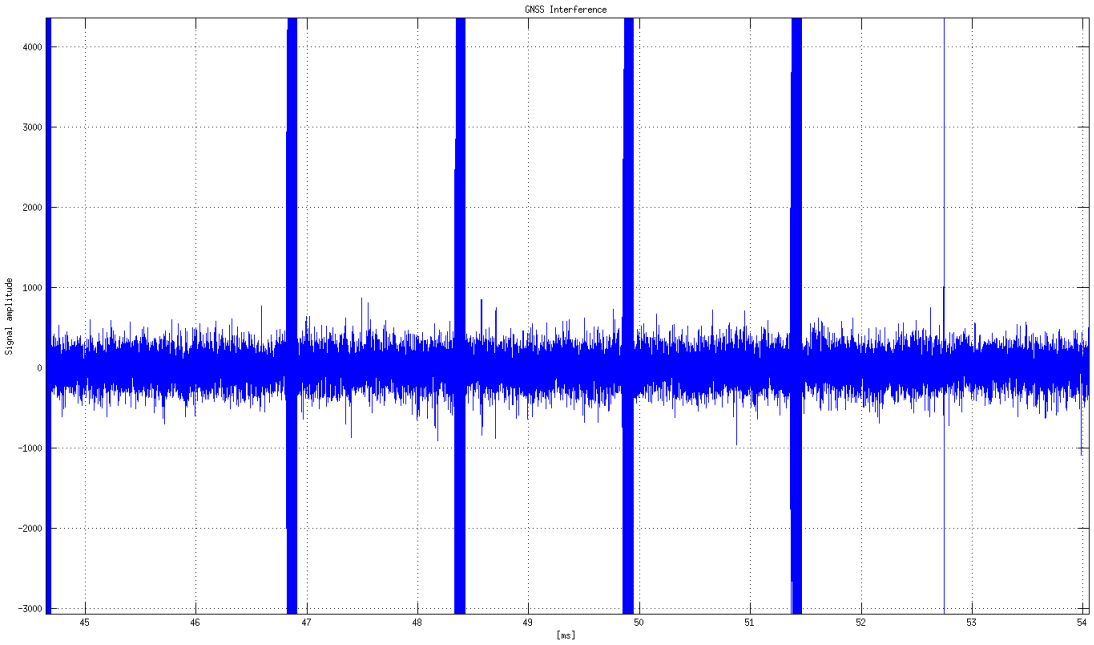

Fig. 4. Galileo E6 pulsed interference periodicity.

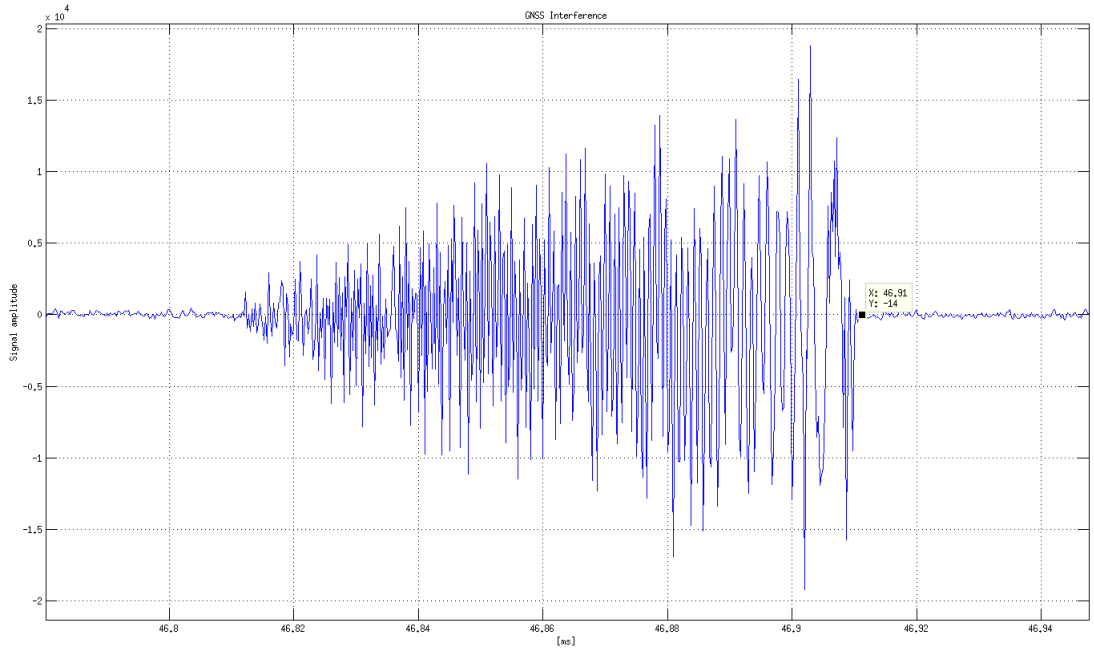

Fig. 5. Galileo E6 single pulse interference time analysis.

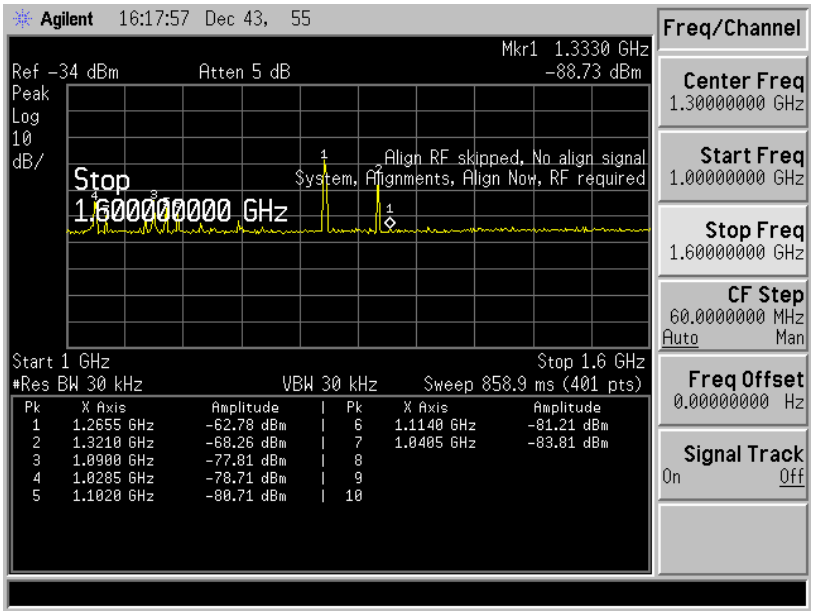

Fig. 6. RF spectrum at the antenna connector.

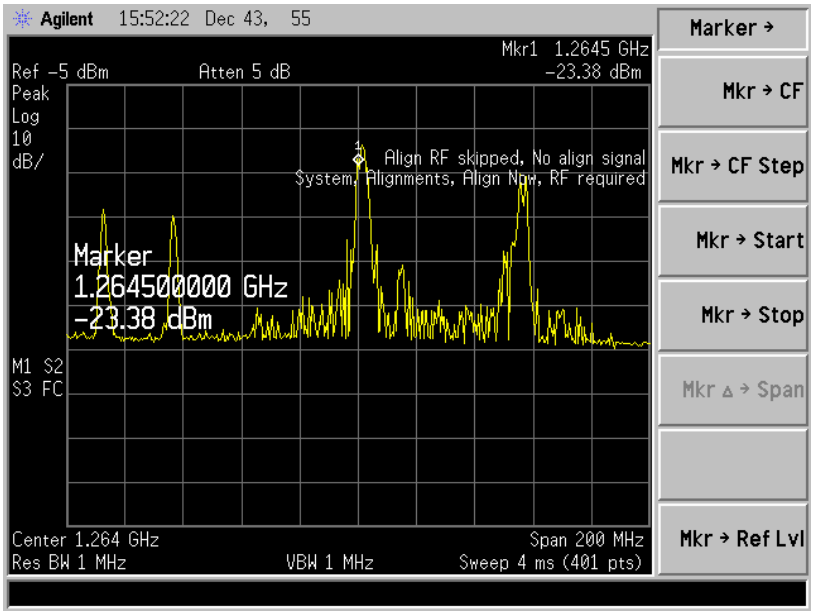

Fig. 7. Spectrum detail of the 1.2655 GHz interference.

Fig. 8. Barcelona L-band ATC primary radar in the GNSS receiver line of sight.

A report was sent on February 2016 by the authors to the Spanish national radio frequency management authorities and an official investigation was performed. Notably, according to the 2016 European Table of Frequency Allocations (see [8], p. 101), the service allocation for the range of $1270 - 1300$ MHz reads:

1. Earth exploration satellite (active)
2. **Radiolocation**
3. Radionavigation satellite (space-to-Earth)
4. Space research (active)
5. Amateur

The listing order indicates the service priority, and thus the ATC radar (a **radiolocation** service) has priority over the radionavigation service. Consequently, the interference will be present until the end of the operational life of the L-band radars and its migration to S-band radars.

Conventional single-frequency GNSS antennas are usually equipped with Surface Acustic Wave (SAW) filters, which provide strong out-of-band attenuation to the interferences and protect the front-end from saturations. However, if the antenna features the E6 band, the radar interference became an in-band interference (seen from the antenna device) that is received with full power into the RF front-end.

General-purpose tunable front-ends integrated circuits, like the Analog Devices AD9361 [12], are typically very sensitive to out-of-band interferences due to the lack of selectivity of their tunable filters. Even by tuning the front-end to the L1/E1 band, it does not protect the input amplifiers and mixers from saturation due to the interference power. The effect are new intermodulation products, which affect all GNSS bands, thus, the out-of-band interference became an in-band interference.

SDR receivers are commonly connected to such front-ends, and thus it is specially important to implement countermeasures to minimize the interference effects. Hereafter, it can be found a brief analysis of the single-antenna interference mitigation techniques, its implementation on an open source GNSS SDR receiver, and its application to the aforementioned ATC radar interference problem. In this article, we purposely omit multi-antenna receiver approaches, which are known to be more involved to design and implement [13].

3. INTERFERENCE SIGNAL MODELS

GNSS is particularly prone to unintended and malicious RFIs due to the extremely low power level of the signal at the user's receiver. Communication systems transmitting at carrier frequencies close to the band of interest are potential source of interferences for a GNSS receiver, and even small leakages out of their allocated bandwidth can be threatening to GNSS signals. Unintentional RFIs events are generally unpredictable. The presence of interfering power can be due to several reasons, but the main effects are caused by harmonics or spurious components generated by intermodulation products in the communication transmitter or in the GNSS receiver front-end. Jamming refers to intentional transmission of RF energy to hinder a navigation service by masking GNSS. According to [14], civil jamming signals are usually classified in two main types:

- CWI. The spectral signature of the CWI consists on a perturbation of a relative small part of the spectrum and can be mitigated by means of a notch filter.
- Short pulsed interferences. These interferences present an instantaneous bandwidth that usually covers the entire GNSS band. Then a well-known algorithm that removes the unwanted signal is the so called pulse blanking filter.

3.1. SIGNAL MODEL

In the presence of jamming or interferences, the baseband signal, $y[n]$, obtained by filtering, down-converting and digitizing the analog signal at the GNSS antenna connector with a sampling frequency f_s, can be defined as

$$y[n] = x[n] + i[n] + \eta[n], \tag{1}$$

where:

- $x[n]$ contains the GNSS constellation signals which will be used for the receiver operations,
- $i[n]$ is the interference signal, particularized depending on the desired interference signal model, and
- $\eta[n]$ is a noise term defined as a complex, circularly symmetric, Additive White Gaussian Noise (AWGN).

Interference Cancellation (IC) consists on removing $i[n]$ from $y[n]$ by means of a signal processing algorithm. The underlying idea seems straightforward, but in practice IC becomes a complicated matter due to the huge variety of interference sources that may coexist within the GNSS signal band. For instance, the interference may be pulsed or may be continuous. In the first case, the period between pulses, time duration, intensity and bandwidth of the pulses can be constant or vary along time. In the second case, the intensity, instantaneous frequency and frequency rate of the interference may also behave randomly. For this reason, there is no "one-fits-all" algorithm for interference mitigation. Furthermore, during last years research literature has been populated with new signal processing techniques that perform many kinds of IC, as reported in [15] and [9], among others. As starting point, a basic model for the interference signal $i[n]$ is presented in the following subsections.

3.2. CONTINUOUS WAVE INTERFERENCES

A single spectral component signal can be expressed as

$$i[n] = A[n]e^{j\varphi[n]}, \tag{2}$$

where $A[n] \in [0, \infty)$ and $\varphi[n] \in (\pi, \pi]$ are two real signals, representing the interference amplitude and phase. Although this model is general, the hypothesis assumed by the single component model is that $i[n]$ is instantaneously narrow band. The instantaneous frequency of a single component signal is defined as the derivative of its phase, which in discrete time is

$$f_i[n] = \frac{\varphi[n] - \varphi[n-1]}{2\pi}. \tag{3}$$

In practice, $A[n]$ has slower dynamics than $f_i[n]$. A useful parameter that quantifies the magnitude of the interference signal is the ratio between the power of the interference signal and the noise power density of the receiver, J/N0. Usual values of this ratio are around 20 to 70 dB-Hz. Figures 9 to 12 show the spectrogram of synthetic jamming signals (J/N0 = 70 dB-Hz) generated in MATLAB, covering from 0 to 8 MHz with linear, quadratic, cubic and sinusoidal frequency modulations.

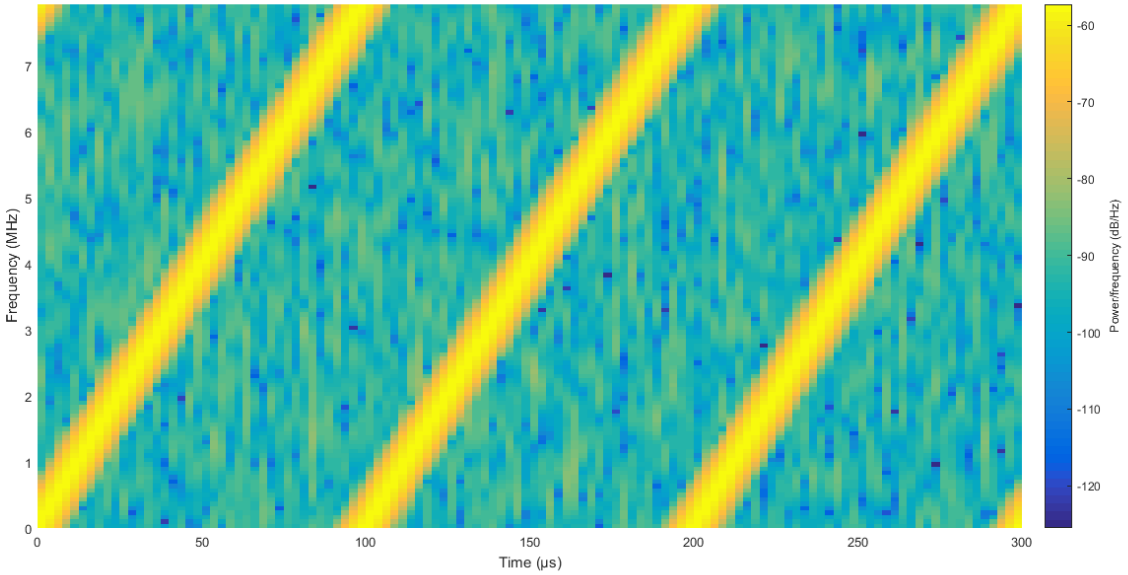

Fig. 9. Linear FM jammer.

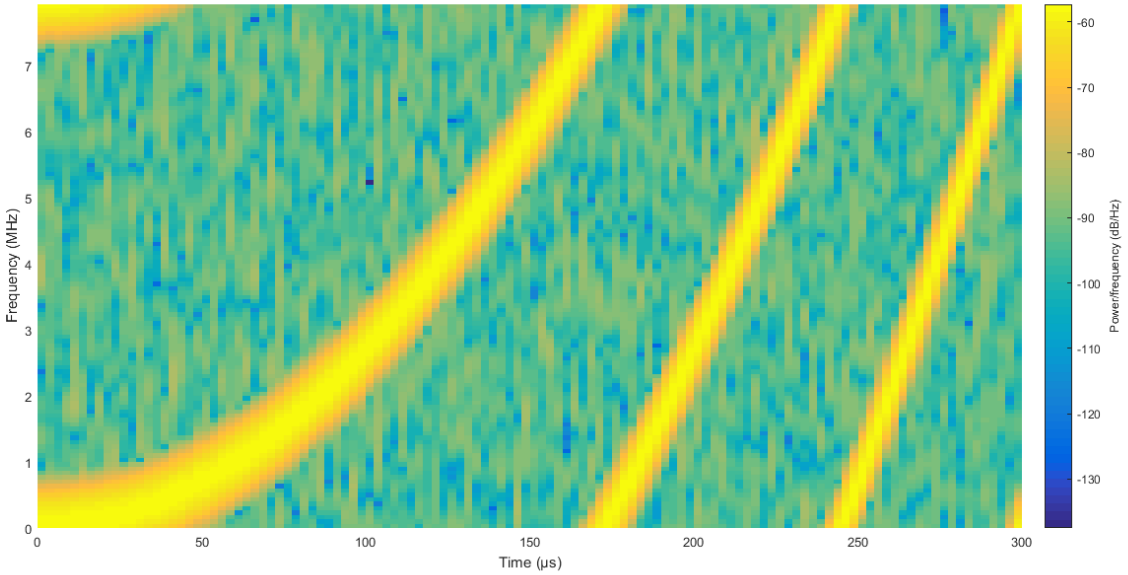

Fig. 10. Quadratic FM jammer.

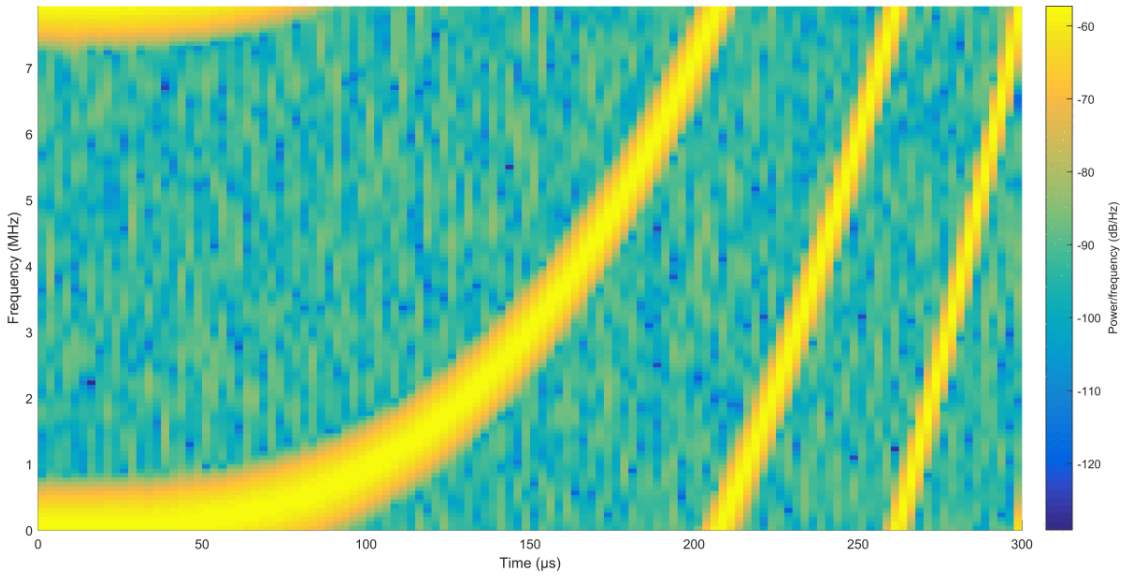

Fig. 11. Cubic FM jammer.

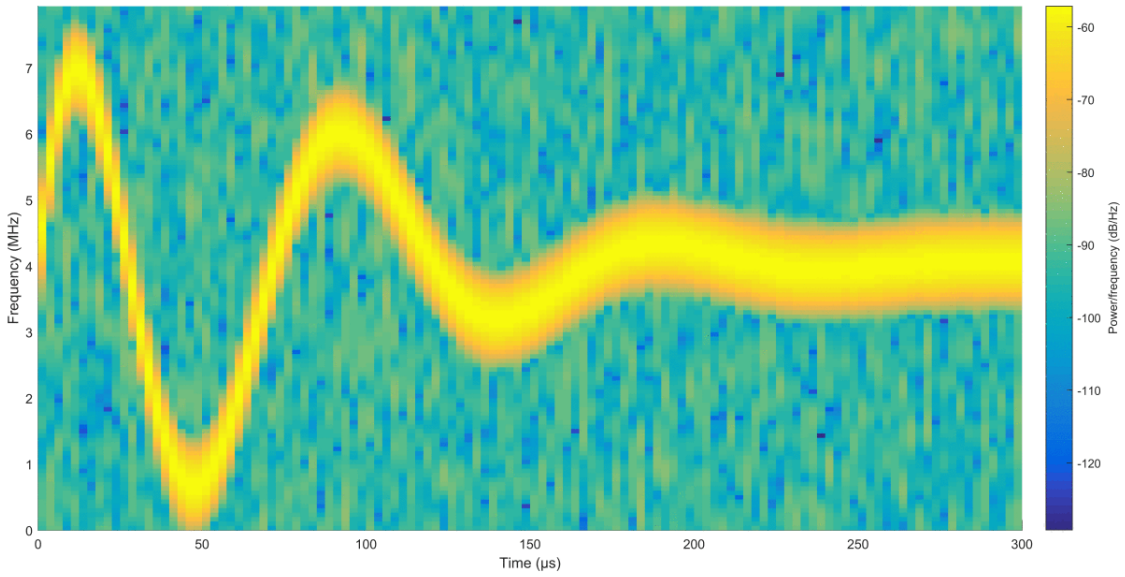

Fig. 12. Sinusoidal amortiguated FM jammer.

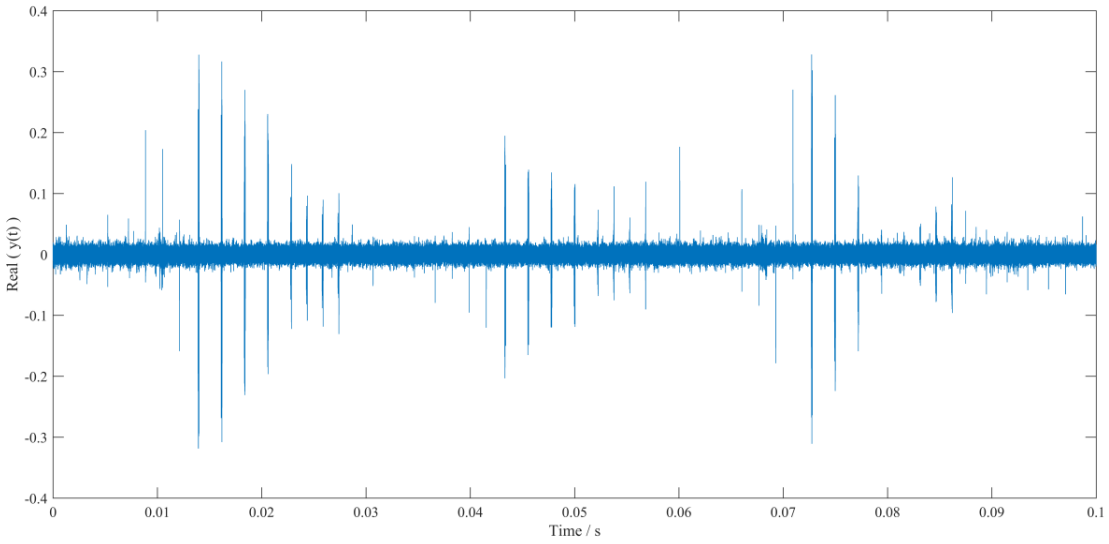

Fig. 13. Time domain plot of a captured GNSS L1/E1 signal interfered by ATC radar pulsed interference.

3.3. PULSED INTERFERENCES

The main particularity of a short time pulsed signal is the broad bandwidth it spans. A proper treatment of these interferences is difficult to be carried out in frequency domain because they often cover the whole receiver's band. Also, the waveform of the pulses is arbitrarily different from one source to other and the time difference between pulses may not be constant. If the pulses are not removed from the original signal, spurious correlation spikes are originated when computing acquisition and tracking of the GNSS signal. The spikes may cause a degradation or even a total loss of the GNSS positioning service. Figure 13 shows an interfered GNSS signal captured by tunning the front-end in Galileo E1 band using the setup described in Section 2. Here, the out-of-band pulses are leaking from Galileo E6 to Galileo E1 due to the front-end poor selectivity and/or intermodulation or saturation problems. Figure 14 represents a single pulse (time duration about 100 s) of the same captured signal.

4. INTERFERENCE DETECTION

The first step of an interference mitigation algorithm consists on determining if the interference is present inside the receiver's band. A simple method from the computational point of view is to compute the input signal power and compare it against a certain threshold. This threshold should be set according to the signal level in absence of the interference signal. Since the power of the GNSS useful signal components at the receiver's antenna is extremely weak (several tens of dB below the background noise), the input signal power when the interference source is switched off is in practice the same as the background noise power, defined as

$$\mathbb{E}\{|y[n]|^2\} \simeq \mathbb{E}\{|\eta[n]|^2\} \simeq \sigma^2. \tag{4}$$

After the ADC step and exploiting the statistical properties of $\eta[n]$ (i.i.d. Gaussian symmetric circular noise), it is possible to set a probability of false alarm, i.e. the probability of detecting the interference even if the jamming signal is absent. Comparing the signal magnitude against the threshold and taking a decision in all the samples is not feasible in real time applications, so the detection algorithm runs on signal segments of L samples. The estimated energy of a signal segment is

$$E_s = \sum_{k=1}^{L} |y[k]|^2, \tag{5}$$

where the random variable $\frac{E_s}{\sigma^2}$ follows a chi-square distribution with $2L$ degrees of freedom. According with the tabulated values of that distribution it is possible to set the threshold with a certain probability of false alarm. When the segment's energy exceeds the detection threshold, then the segment is processed with the interference mitigation algorithm. Note that σ^2 should

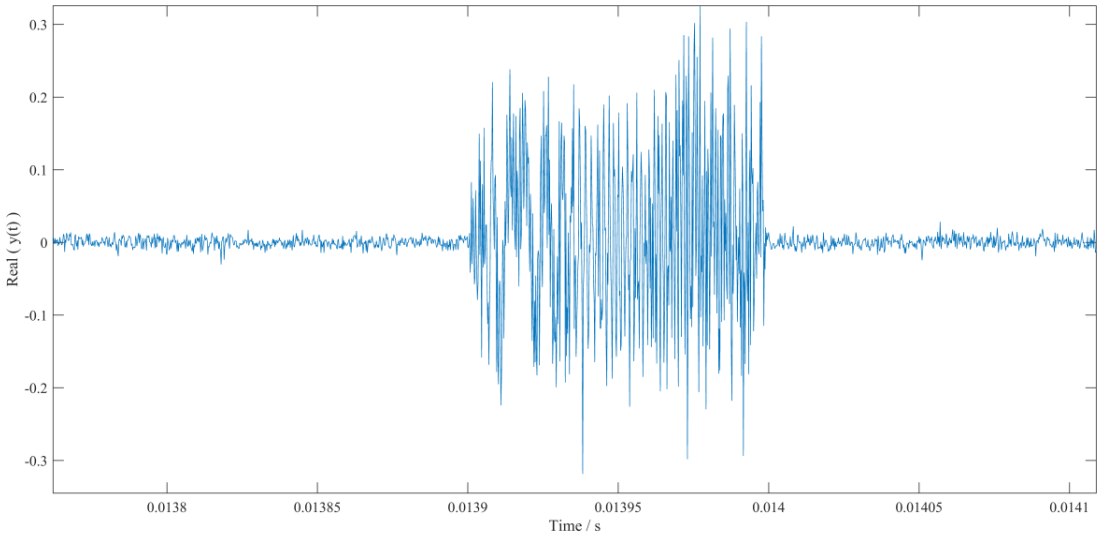

Fig. 14. ATC radar pulse waveform leaked from E6 to L1/E1 frequency.

be estimated by a noise floor power estimation method. With the purpose of minimizing the random effects, several noise power estimations are averaged on consecutive signal segments. In addition, as the receiver background noise may change over time, the estimation of σ^2 is performed periodically.

In this sense, the minimum signal length to be processed (filtered by a mitigation input filter) is one signal segment because the detection of an interference affects to the entire segment. Figure 15 summarizes the underlying idea of the noise power estimation and filtering epochs. Note that the length of these epochs may be different. In practice, filtering epochs are much longer than noise power estimation epochs.

5. CONTINUOUS WAVE INTERFERENCE MITIGATION

In the literature it can be found several signal processing techniques to mitigate CW interferences. For example, transform domain excision techniques project the input signal onto a domain where the interference signal assumes a sparse representation [15]. The interference signal is then estimated from the most powerful coefficients of the transformed domain representation. The interference signal is removed in the transformed domain, and the GNSS signal is obtained by anti-transforming the mitigated signal. Transform domain excision techniques are, however, computationally demanding. Other works are focused on Finite Impulse Response (FIR) filters and highlights the limitations of these types of filters due to the required high order of the filter. In this work, the chosen implementation is a multi-state Infinite Impulse Respone (IIR) Notch filter [16].

5.1. MULTI-STATE ADAPTIVE NOTCH FILTER

Single components can be generated by a first order recurrence equation

$$i[n] = a[n]i[n-1], \tag{6}$$

where $a[n]$ is a time varying coefficient that depends on the jamming estimated parameters:

$$a[n] = \frac{A[n]}{A[n-1]} e^{j(\phi[n] - j\phi[n-1])} = \frac{A[n]}{A[n-1]} e^{j2\pi f_i[n]}. \tag{7}$$

The single component assumption and the recurrence equation allow the prediction of $i[n]$ from the past sample. This principle is exploited in a single pole, single zero IIR. Notch Filter whose transfer function is defined as

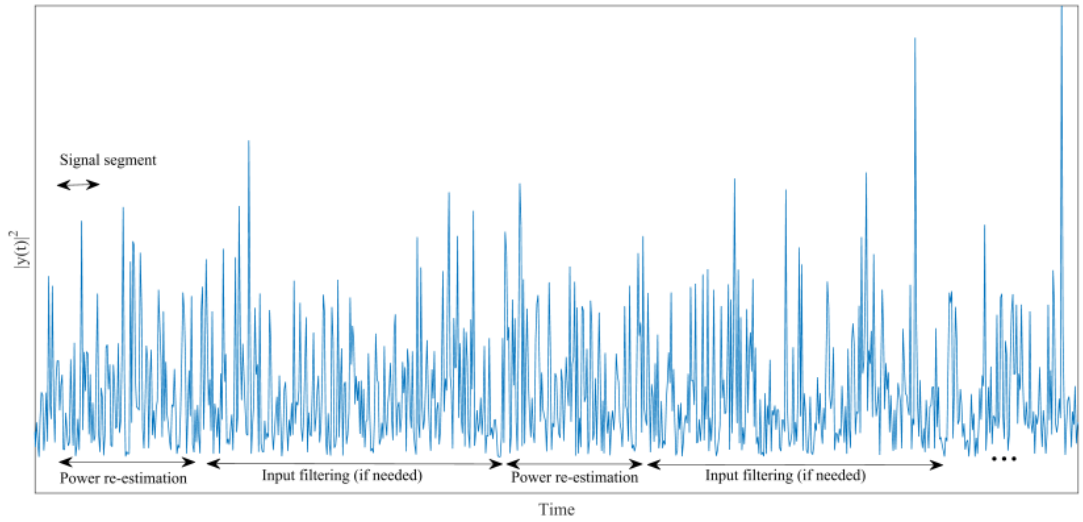

Fig. 15. Squared magnitude of a GNSS signal segment in absence of interference and the interference detection and mitigation processes.

$$H_n(z) = \frac{1 - z_0[n]z^{-1}}{1 - kz_0[n]z^{-1}}, \tag{8}$$

where $z_0[n]$ is the complex zero of the filter and k is the pole contraction factor, ranging from 0 to 1. The pole contraction factor determines the bandwidth of the Notch filter, the closer to 1 the smaller the filter bandwidth. The aim of the Notch filter is to eliminate jamming signals who are instantaneously narrowband and, also, their instantaneous frequency changes along time. Under these assumptions, the zero of the Notch filter must be adaptive.

At this point, an additional task must perform the Notch filter: to track (and estimate) the instantaneous frequency of the jamming signal. Instantaneous frequency can be estimated by means of diverse methods. At a first approach, FFT based algorithms seem a good solution, but, despite the efficiency of FFT, it is very computer consuming for real time solutions. In addition, if the frequency change rate of the FM modulation of the jammer is fast respect to the duration of the FFT, what we obtain is a bad estimation of the instantaneous frequency. Other valid estimators are Frequency Lock Loop (FLL) and the stochastic gradient which are relatively less computational demanding. Kalman filter has been also suggested in the literature for tracking the instantaneous frequency. All these estimation methods are prone to fail when non-linear variations or discontinuities appear on the jammer FM frequency.

In this work, a simple single-sample Prony's frequency estimator has been selected and the interference frequency is estimated as

$$\hat{f}_i[n] = \frac{1}{2\pi}\angle\{y[n]y^*[n-1]\}. \tag{9}$$

In Eq. 8, $z_0[n]$ coefficient of the filter determines the attenuated Notch frequency and is set to $z_0[n] = e^{j2\pi\hat{f}_i[n]}$. Note that Prony's frequency estimator is computed in every signal sample and provides the highest responsiveness of the filter to frequency changes. Furthermore, the filter must detect the presence or absence of CW interferences. In case of absence, the filter should behave as a pass-through filter. The block diagram of the filter is represented in Fig. 16.

The energy detector works as explained in this section. Respect to the background noise power estimation, it is performed by means of a noise floor power estimator. In an SDR environment, the power estimation can be implemented using a function provided by the GNU Radio Vector-Optimized Library of Kernels (VOLK) library [17]. It computes the mean value of the

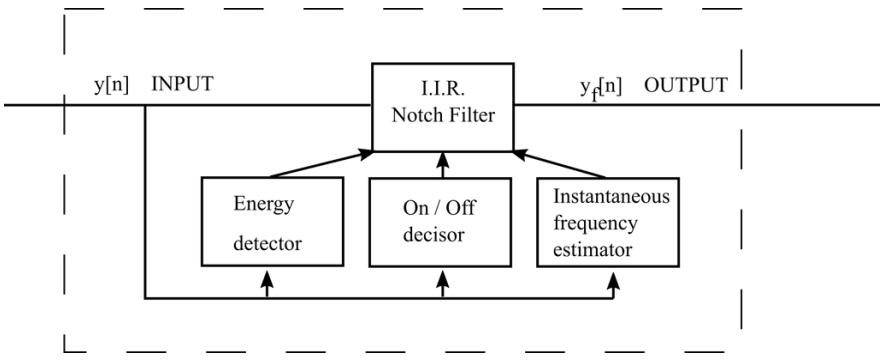

Fig. 16. Block diagram of the adaptive Notch filter.

power spectral density of the analyzed signal segment and identifies the points above a certain configurable threshold (in the captured signal, the threshold was set to 15 dB, determined empirically by the authors). Then, the mean value of the power spectral density is recalculated excluding the most intense points. The main advantage of this noise floor estimator is that the filter is able to estimate the noise power even in presence of CW interferences. Furthermore, two implementations of the adaptive Notch filter were coded.

The first one is the *Notch_Filter* implementation and works as detailed in this section. The second one is the *Notch_Filter_Lite* implementation were the user can choose the updating rate (in Hz) of the filter central frequency. The latter implementation requires lower computational resources since the Prony's estimation is no longer performed sample by sample. *Notch_Filter_Lite* filter updating rate must be according to the variation rate of the jammer FM. Slow variations in the jammer frequency are well tracked by a slow updating rate. However fast variations in the jammer frequency are not followed by a slow updating rate. In this implementation, the maximum updating rate available is one update per signal segment, this is to say, eq 10. Being fs the sampling frequency and L the number of samples per signal segment. The pole contraction factor, k, should also be reduced (it implies a wider eliminated band) with respect to the *Notch_Filter* implementation since a wider eliminated bandwidth will also eliminate the jamming signal in case of a slower coefficient updating rate. It must be considered that an excessively wide rejection band removes, also, part of the useful GNSS signal.

5.2. NOTCH FILTER RESULTS

Authors have not access to a captured GNSS signal contaminated by a real CW jammer. However, for the experiment, it is used a clean captured GNSS signal of 100 seconds of duration. This signal was recorded in baseband at 4 Msps and the data type is interleaved integer shorts, this is, 16-bit signed integers for the In-Phase samples and 16-bit signed integers for the Quadrature samples. The signal was contaminated by means of a jamming generator coded in MATLAB that generates a configurable FM signal. The configurable parameters are the J/N0, the kind of FM modulation (linear, quadratic, cubic, sinusoidal or a spline function) and the possibility of generating discontinuities in the FM modulation as well as the option to randomly switch on and off the jammer. The synthetically contaminated signals were recorded in *gr_complex* data type (interleaved I-Q 32-bit float numbers).

Fig. 17 represents the spectrogram of the original signal. Note that a spurious tone at 0.6 MHz is present generated by a front-end local oscillator leakage. In any case, the power of this tone is low enough in the sense that it does not cause any considerable perturbation on the signal. For instance, when running the GNSS-SDR receiver with the *Pass_Through* input filter implementation, the receiver processes the signal properly.

Some contaminations of the original signal were performed for testing purposes. Following, the best and worst cases are presented in terms of the FM modulation. The best one consists on a linear FM modulation: the instantaneous frequency sweeps the 4 MHz bandwidth linearly. The worst case is a spline modulation: the instantaneous frequency follows a random spline function covering uniformly all the receiver's bandwidth. Also, frequency jumps are present in both signals. The contaminated signals where filtered with the *Notch_Filter* input filter implementation on the GNSS-SDR testbed and their corresponding

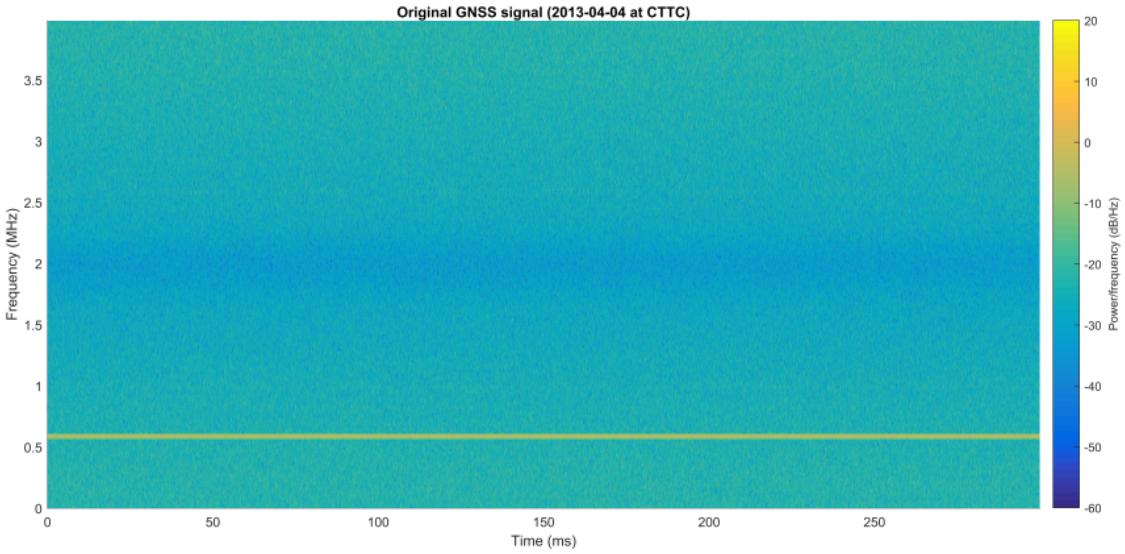

Fig. 17. Spectrogram of an interference-free captured GNSS signal.

input/output spectrograms are represented in Fig. 18 and Fig. 19 respectively for the linear FM jammer and Fig. 20 and Fig. 21 respectively for the spline FM jammer.

Note that an unexpected alias of the CW interference is generated by the Notch filter. A concept test was performed on MATLAB to debug the artifact and the alias did not appear. A possible cause may be related to quantification errors in the filter or a quantification error in the *atan2* VOLK kernel. The *atan2* function is used in order to obtain the Prony's instantaneous frequency estimation as already mentioned. In any case, these alias present a power on the order of the 0.6 MHz spurious and do not mask the useful GNSS signal. By means of the *Notch_Filter* implementation, the GNSS-SDR receiver is able to acquire, track and decode the GNSS (GPS in this case) signal correctly. The time to first fix in the case of contaminated signals matches with the case of the original signal. Note that when processing the contaminated signals with the *Pass_Through* input filter implementation any position fix was obtained: tracking losses in all the channels were constant.

An example of the Notch_Filter_Lite implementation is shown in Fig. 22, where the same signal as in Fig. 21 is filtered with a coefficient updating frequency rate of 50 kHz. The CW interference has been attenuated about 20 dB, but however its intensity is still high and causes severe tracking problems. The maximum value of the coefficient updating rate is limited by the signal segment length. In order to increase the coefficient updating rate, it is needed to decrease the length of the signal segment. But decreasing the length of the signal segment gets a worse noise power estimation because of the resolution loss of the Fast Fourier Transform (FFT) and this is translated into a higher probability of error in the interference detection block. When errors take place in the interference detection block, may happen that the interference is not detected and, thus, it is not filtered out. Summarizing, *Notch_Filter_Lite* provides similar results to *Notch_Filter* implementation when the FM of the jammer changes slowly enough. The length of the signal segment is not recommended to be under 64 points in any case for obtaining a good estimation of the power noise floor.

The pole contraction factor was set to 0.9 in all the presented cases. Usual values for this parameter are around 0.8 and 0.9. The performances of the *Notch_Filter* implementations were tested with different data types (i.e. *ishort*, *gr_complex*). When working with *ishort*, it was noticed that, although the filter eliminates properly the CW interference, the remaining signal was completely corrupted because of the quantification error. When digitizing contaminated signals with usual values of J/N0, the resulting discrete signals consist only on the quantification of the interference: the weak GNSS signal is then removed from the discrete signal. By means of floating point samples (*gr_complex* type), the quantification error is reduced and both the interference and the GNSS signal are well captured.

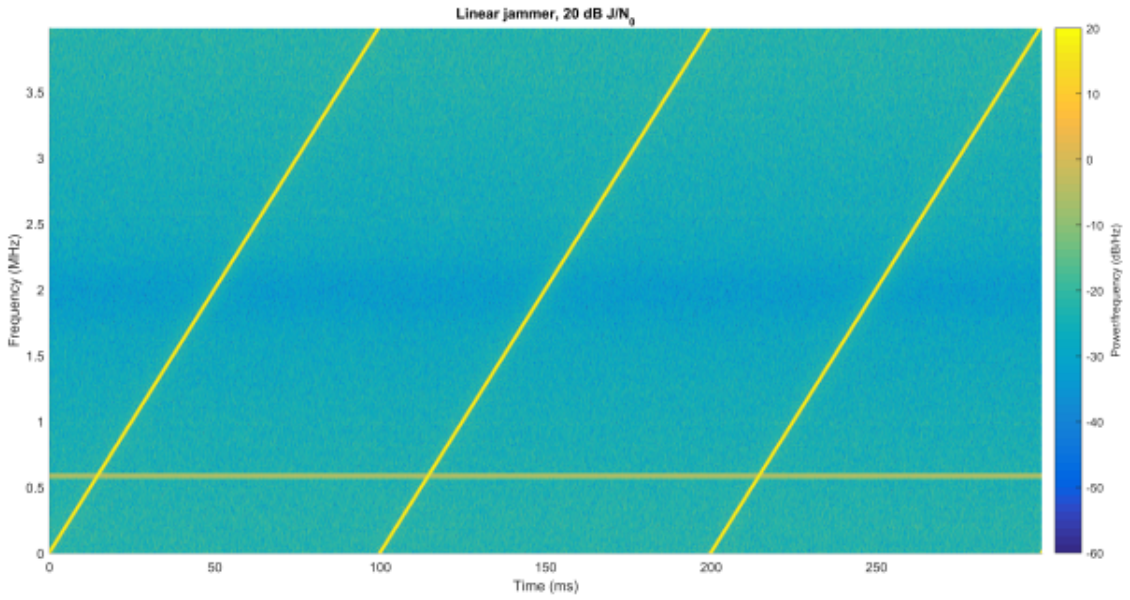

Fig. 18. Spectrogram of the contaminated GNSS signal with a linear FM jammer modulation before the interference filter.

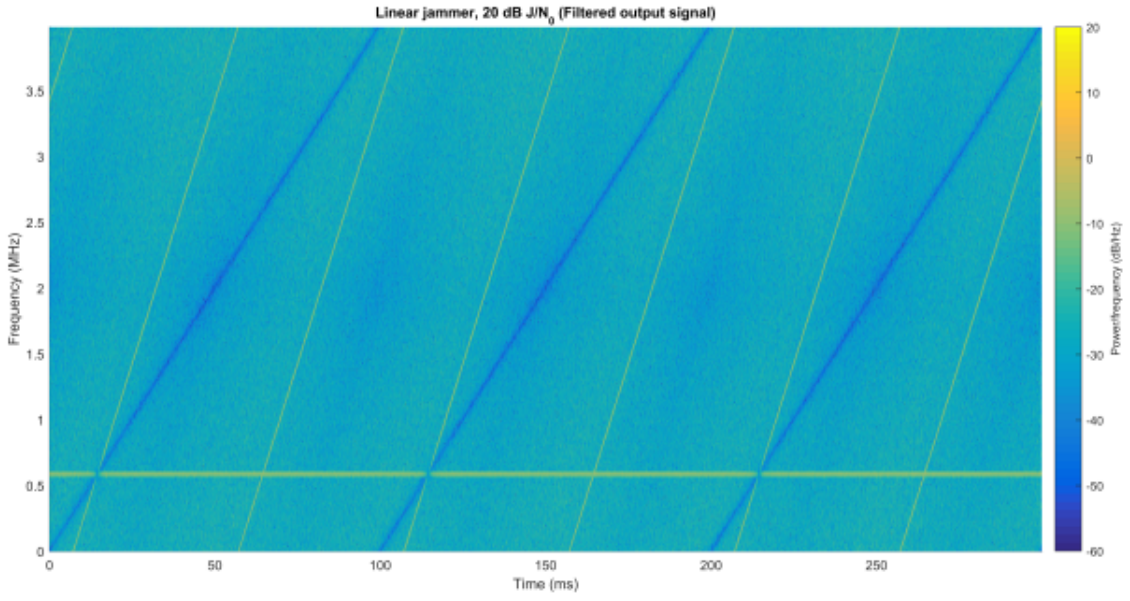

Fig. 19. Spectrogram of the contaminated GNSS signal with a linear FM jammer modulation after the interference filter.

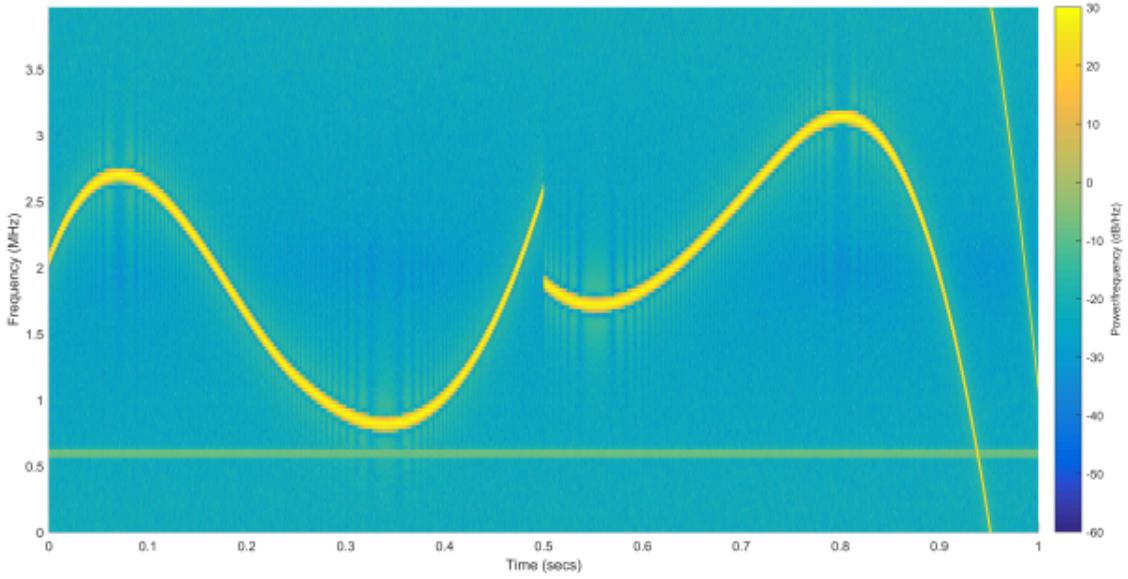

Fig. 20. Spectrogram of the contaminated GNSS signal with a spline FM jammer modulation before the interference filter.

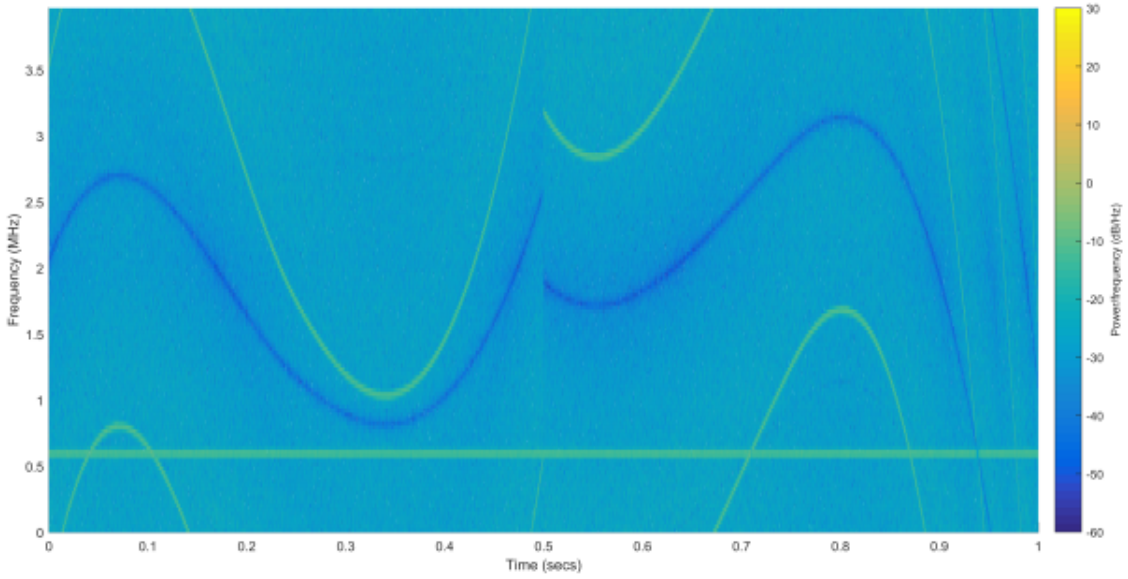

Fig. 21. Spectrogram of the contaminated GNSS signal with a spline FM jammer modulation before the interference filter.

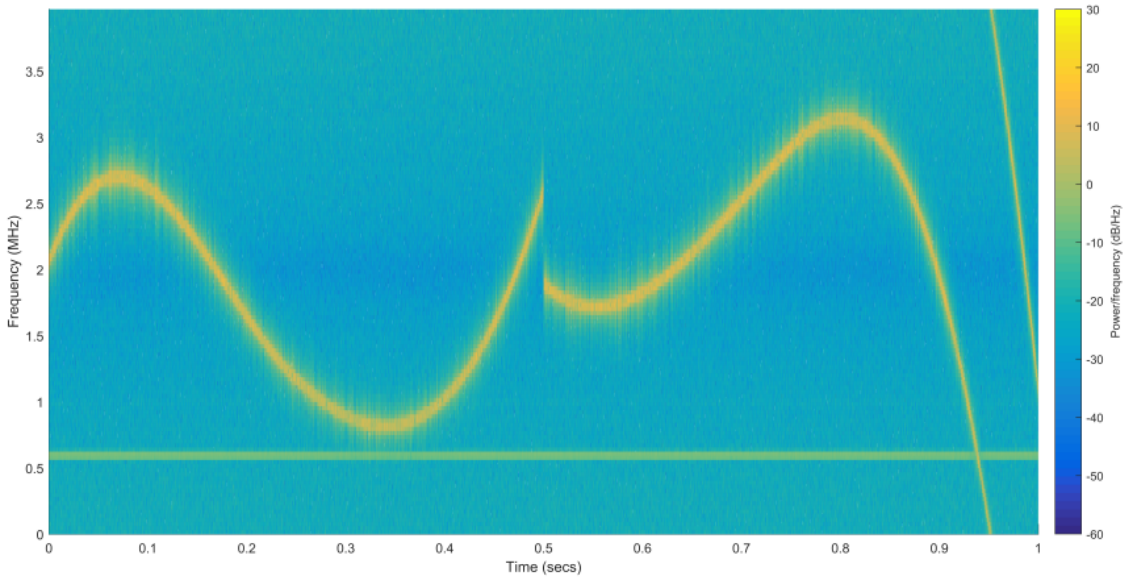

Fig. 22. Spectrogram of the filtered signal with the Notch Filter Lite implementation: spline FM jammer modulation.

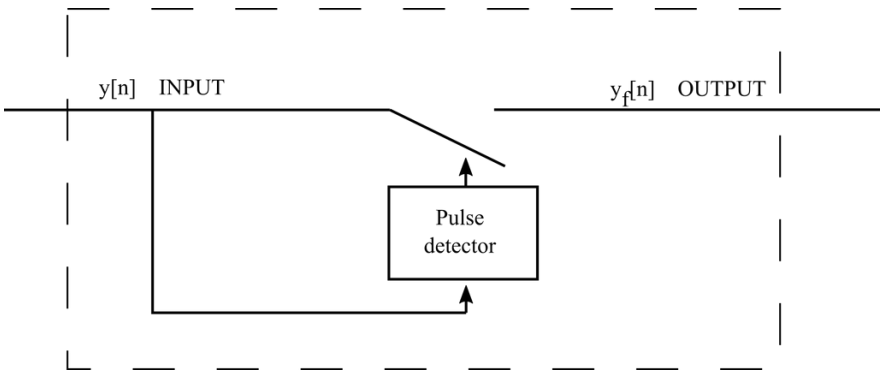

Fig. 23. Block diagram of the Pulse Blanking filter.

6. PULSED INTERFERENCE MITIGATION

The principle of digital pulse blanking is simple. It relies on the fact that pulses are short and have large amplitude compared to the noise level. In essence, the pulse blanking unit immediately triggers whenever a pulse arrives at the receiver's input and prevent the pulse from passing into the tracking (or acquisition) blocks. While the pulse blanking filter is active, the signal at the output is set to 0. The pulse blanking unit must be highly responsive by design and tuned such that the input signal is only blanked out for the duration of the pulse. Taking a pulse duty cycle of 5%, as an example, the effect of the pulse blanking unit on the C/N0 is only reduced by 0.2 dB-Hz [9].

6.1. PULSE BLANKING FILTER

The basic principle of a Pulse Blanking filter is illustrated in Fig. 23. If the input signal has a squared magnitude within a signal segment greater than the blanking threshold γ, then the output signal is set to zero. Otherwise, the output is equal to the input. Replacing the corrupted samples by zero ensures that correlation values are minimally distorted.

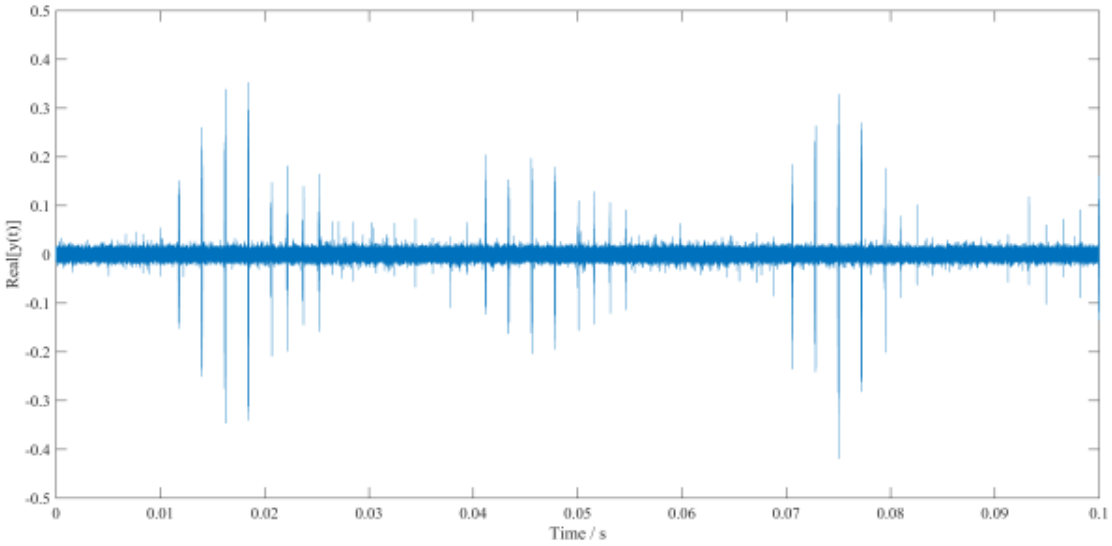

Fig. 24. Time domain plot of a captured GNSS L1/E1 signal interfered by ATC radar pulses.

$$y_f[n] = \begin{cases} y[n] & \text{if } E_s < \gamma \\ 0 & \text{if } E_s > \gamma \end{cases} \tag{10}$$

The blanking threshold γ is set according to this section. In a first implementation of the filter, the noise power estimation was carried out by the pulse clipping technique. Noise floor determination can be corrupted if the estimation is done using pulsed samples. If it is not possible for the noise floor estimation to be aware of periods without pulses, pulse clipping seems a good idea. Pulse clipping replaces the samples higher than a certain value by simulated noise samples. This algorithm requires the user to introduce the clipping threshold as an initial parameter in the configuration file. However, this threshold is not straightforward to know a priori and the overall pulse clipping algorithm introduces a certain extra computational charge. On the contrary, the final implemented noise estimation method is the simplest algorithm. It computes the arithmetic mean of the squared magnitude input signal during the estimation epoch (several milliseconds of signal). The short pulses, which may be present during the estimation process, are only a few samples inside the total samples and do not increase the noise power estimation significantly.

A validation of this algorithm was performed after the implementation of the full pulse blanking block. The means of the noise floor estimations in the original pulsed signal and in the blanked signal were computed and the relative difference was around 1%.

6.2. PULSE BLANKING RESULTS

The pulse blancking algorithm implementation was tested using 53 seconds of a signal captured by tunning the front-end in the Galileo E1 band using the setup described in Section 2. The signal was in baseband, at a sampling frequency of 5Msps and the data type was *gr_complex* (interleaved I-Q 32-bit float numbers). First of all, the signal was analyzed in time domain trying to find any temporal pattern. Neither the pulse repetition frequency (number of pulses per second) nor the pulse intensity were constant along the time. The time duration of the pulses is about 100 s. Then, the signal was filtered with the *Pulse_Blanking* input filter implementation on GNSS-SDR. An extract of the input and output signals in time domain is represented in Fig. 24 and Fig. 25, respectively.

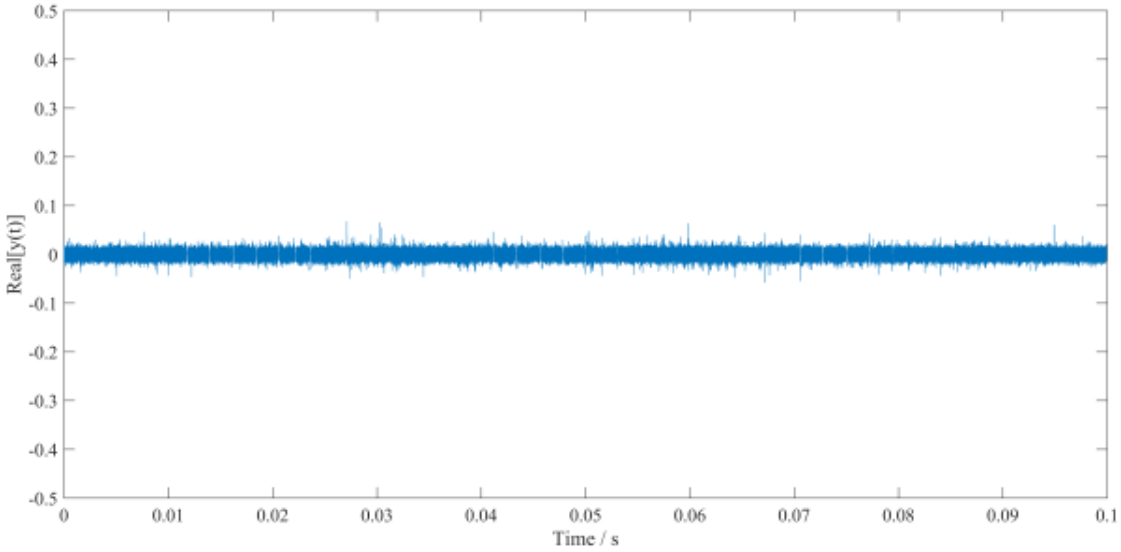

Fig. 25. Time domain plot of a captured GNSS L1/E1 signal interfered by ATC radar pulses after the implemented pulse blanking filter.

By using the filter, the quality of the signal was considerably improved. Without the filter, the receiver was not able to operate: continuously got tracking lock losses because the pulses produced spikes in the Early - Prompt - Late correlators. Figure 26 shows the tracking results when no input filter is configured. No navigation messages were decoded.

Figure 27 shows the tracking results when the Pulse Blanking filter is set with a low probability of false alarm (0.001). This implies a high blanking threshold value. In this case, the receiver is able to decode the navigation messages and the time to first fix is 42 seconds. Early - Prompt - Late correlators behave normally except in 17 correlator outputs where spikes due to non-blanked pulses still appeared.

Finally, Fig. 28 shows the tracking results when the Pulse Blanking filter is set with a higher probability of false alarm (0.04). In this case, the blanking threshold value is low and all the pulses except one around the second 32 are blanked. Due to the high value of probability of false alarm, around 4% of the useful GNSS signal is blanked in absence of pulsed interference. Despite of that, the receiver operates normally and the time to first fix was also 42 seconds. Early - Prompt - Late correlators outputs are cleared of spikes except one (the non-blanked pulse at second 32).

7. GNSS-SDR CONFIGURATION PARAMETERS

The implementation of the selected interference mitigation algorithms is open source and it is currently available in a GitHub repository [18]. It is scheduled to be merged with GNSS-SDR main branch by the end of 2017. Table 2 shows the configuration file parameters required to instantiate the *InputFilter* blocks using GNSS-SDR standard configuration files (see GNSS-SDR website for more information of how to use and configure the receiver [10]).

8. CONCLUSIONS

In this work, the authors presented a serious threat to the Galileo E6 users caused by an in-band L-band ATC radar pulsed interference which is currently *authorized* by the ITU radio regulations in Europe. This paper reports the complete sequence of facts in a real environment, from the interference detection, time/frequency analysis, source identification and location to the mitigation of its effects by implementing a real-time pulse blanking algorithm in an open source, software defined GNSS receiver. The vulnerability of general purpose front-ends to strong out-of-band interferences due to lack of selectivity and component non-linearities was also evidenced, which is specially concerning for SDR receiver users. In order to assess the

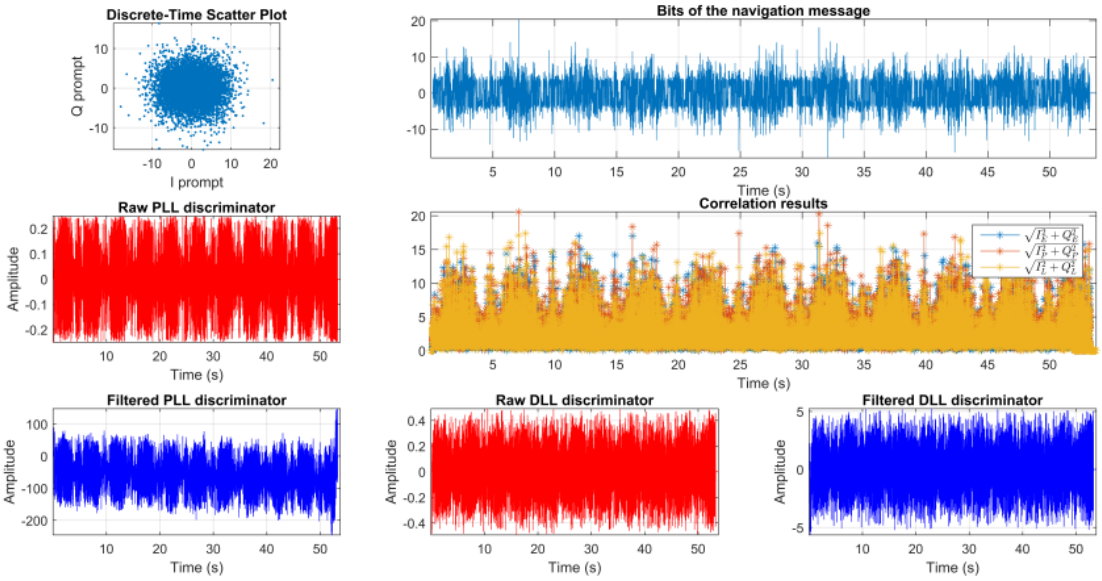

Fig. 26. Tracking plot with Pass_Through input filter implementation.

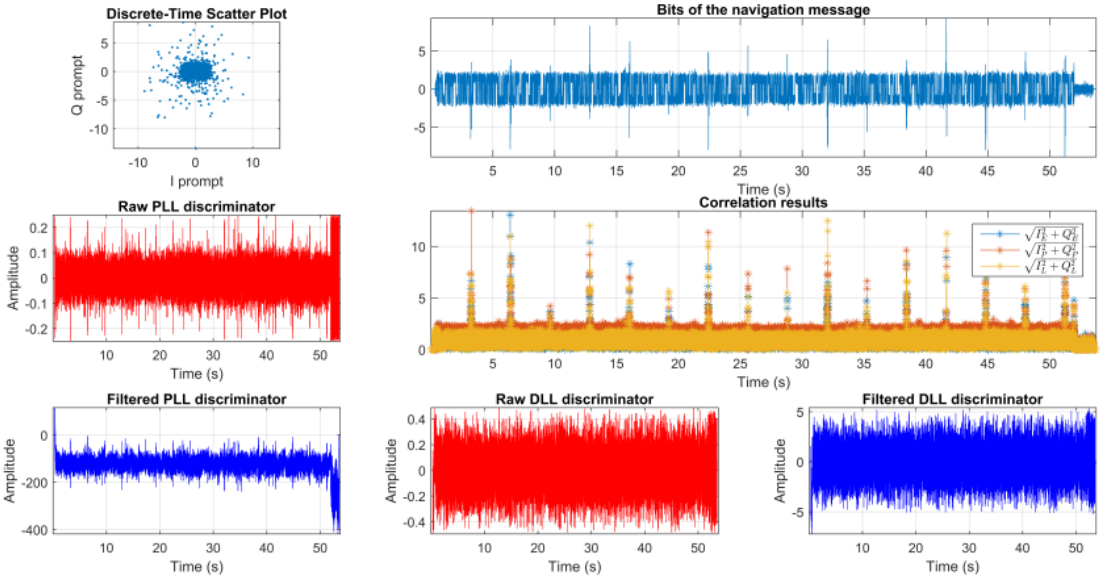

Fig. 27. Tracking plot with Pulse_Blanking input filter implementation and probability of false alarm = 0.001.

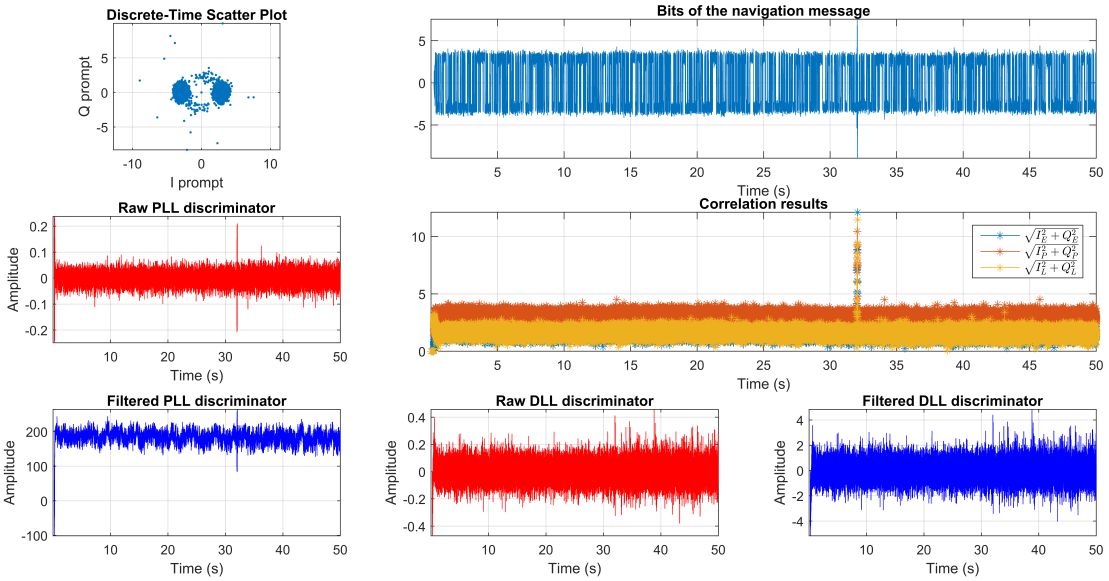

Fig. 28. Tracking plot with Pulse_Blanking input filter implementation and probability of false alarm = 0.04.

Table 1. Notch filter configuration.

Parameter	**Description**	**Required**
implementation	Notch_Filter	Mandatory
p_c_factor	Pole contraction factor of the filter [0 to 1]. The higher the value the lower the filter bandwidth. It defaults to 0.9	Optional
pfa	Probability of false alarm. It defaults to 0.001	Optional
length	Number of signal samples per analysis segment. It defaults to 32	Optional
item_type	Data type. This implementation only accepts gr_complex. It defaults to gr_complex	Optional
segments_est	Number of signal segments in a noise floor estimation epoch. It defaults to 12500	Optional
segments_reset	Number of signal segments between two consecutive noise floor estimations. It defaults to 5000000	Optional Optional
dump	Flag for storing the signal at the filter output in a file. It defaults to false	Optional
dump_filename	If dump is set to true, path to the file where output data is stored	Optional

Table 2. Notch filter lite configuration.

Parameter	**Description**	**Required**
implementation	Notch_Filter	Mandatory
p_c_factor	Pole contraction factor of the filter [0 to 1]. The higher the value the lower the filter bandwidth. It defaults to 0.9	Optional
pfa	Probability of false alarm. It defaults to 0.001	Optional
coeff_rate	Updating rate of the filter coefficients in Hz. It defaults to tenth the sampling frequency	Optional
length	Number of signal samples per analysis segment. It defaults to 32	Optional
item_type	Data type. This implementation only accepts gr_complex. It defaults to gr_complex	Optional
segments_est	Number of signal segments in a noise floor estimation epoch. It defaults to 12500	Optional
segments_reset	Number of signal segments between two consecutive noise floor estimations. It defaults to 5000000	Optional Optional
dump	Flag for storing the signal at the filter output in a file. It defaults to false	Optional
dump_filename	If dump is set to true, path to the file where output data is stored	Optional

Table 3. Pulse blanking filter configuration.

Parameter	**Description**	**Required**
implementation	Pulse_Blanking_Filter	Mandatory
pfa	Probability of false alarm. It defaults to 0.04	Optional
length	Number of signal samples per analysis segment. It defaults to 32	Optional
item_type	Data type. This implementation only accepts gr_complex. It defaults to gr_complex	Optional
segments_est	Number of signal segments in a noise floor estimation epoch. It defaults to 12500	Optional
segments_reset	Number of signal segments between two consecutive noise floor estimations. It defaults to 5000000	Optional Optional
dump	Flag for storing the signal at the filter output in a file. It defaults to false	Optional
dump_filename	If dump is set to true, path to the file where output data is stored	Optional

interference protection options of an receiver, three new input filter blocks have been implemented and integrated into the open source GNSS-SDR receiver. These signal processing blocks aim to mitigate two common types of interferences: continuous wave FM modulated and short-time pulsed ones. Two blocks deal with the CW interferences, implementing an adaptive Notch filter interference canceler. The first implementation performs a very effective mitigation of CW interferences even in cases of very fast instantaneous frequency variations. The second implementation is a less computing resources solution that is valid only when the instantaneous frequency changes relatively slowly. The third block is a Pulse Blanking filter that mitigates pulsed interferences. Both algorithm implementations were tested with real GNSS signals. The pulse blanking algorithm implementation demonstrated excellent performance against the radar pulses and the receiver was able to operate normally in this harsh interference environment.

ACKNOWLEDGEMENTS

This work has been supported by the Spanish Ministry of Economy and Competitiveness through project TEC2015-69868-C2-2-R (ADVENTURE) and Google Inc. via the Google of Summer of Code 2017 Program.

REFERENCES

[1] M. G. Amin, P. Closas, A. Broumandan, and J. L. Volakis, "Vulnerabilities, threats, and authentication in satellite-based navigation systems [scanning the issue]," *Proceedings of the IEEE*, vol. 104, no. 6, pp. 1169–1173, 2016.

[2] M. De Angelis, R. Fantacci, S. Menci, and C. Rinaldi, "Analysis of air traffic control systems interference impact on galileo aeronautics receivers," in *IEEE International Radar Conference, 2005.*, May 2005, pp. 585–595.

[3] G. G. Xingxin, "DME/TACAN Interference and its Mitigation in L5/E5 Bands," in *Proceedings of the 20th International Technical Meeting of the Satellite Division of The Institute of Navigation (ION GNSS 2007)*, Fort Worth, TX, September 2007, pp. 1191–1200.

[4] Helios and Eurocontrol, "FCI Technology Investigations: L Band Compatibility Criteria and Interference Scenarios Study," *Deliverable C5: Compatibility criteria and test specification for GNSS*, May 2009.

[5] B. Motella, A. Tabatabaei Balaei, and L. Lo Presti, "Characterization of Radar Interference Sources in the Galileo E6 Band," *The Journal of Aerospace Science, Technology and Systems, Aerotecnica Missili & Spazio*, vol. 1, no. 88, pp. 42–53, 2016.

[6] European GNSS Agency, *GSA Today Newsletter, Galileo Commercial Service Implementing Decision enters into force*, February 2017, https://www.gsa.europa.eu/newsroom/news/galileo-commercial-service-implementing-decision-enters-force.

[7] International Telecommunications Union (ITU), Geneva, *ITU Radio Regulations 2016*, 2016, http://www.itu.int.

[8] European Conference of Postal and Telecommunications Administrations (CEPT) Working Group Frequency Management, European Common Allocation (ECA), *European Table of Frequency Allocations in the range 8.3 kHz to 3000 GHz*, June 2016.

[9] D. Borio, "Swept GNSS jamming mitigation through pulse blanking," in *Proc. European Navigation Conference (ENC)*, Helsinki, 2016.

[10] "GNSS-SDR website," Source code available at https://github.com/gnss-sdr/gnss-sdr Accessed on Feb. 27, 2017, http://gnss-sdr.org.

[11] J. Arribas, C. Fernández–Prades, and P. Closas, "GESTALT: A testbed for experimentation and validation of GNSS software receivers," in *Proc. 28th Int. Tech. Meeting Sat. Div. Inst. Navig.*, Tampa, FL, Sep. 2015, pp. 3222–3234.

[12] Analog Devices, *AD9361 RF Agile Transceiver*, September 2017, http://www.analog.com/en/products/rf-microwave/integrated-transceivers-transmitters-receivers/wideband-transceivers-ic/ad9361.html.

[13] C. Fernández-Prades, J. Arribas, and P. Closas, "Robust GNSS Receivers by Array Signal Processing: Theory and Implementation," *Proceedings of the IEEE*, vol. 104, no. 6, pp. 1207–1220, June 2016.

[14] R. H. Mitch, R. C. Dougherty, M. L. Psiaki, S. P. Powell, B. W. O'Hanlon, J. A. Bhatti, and T. E. Humphreys, "Signal Characteristics of Civil GPS Jammers," in *Proceedings of the ION GNSS 2011, Portland, Oregon (USA)*, September 2011.

[15] D. Borio, L. Camoriano, S. Savasta, and L. L. Presti, "Time-Frequency Excision for GNSS Applications," *IEEE Systems Journal*, vol. 2, no. 1, pp. 27–37, March 2008.

[16] D. Borio, "A multi-state notch filter for gnss jamming mitigation," in *International Conference on Localization and GNSS 2014 (ICL-GNSS 2014)*, June 2014, pp. 1–6.

[17] "GNU Radio vector-optimized library of kernels (VOLK)," http://gnuradio.org/redmine/projects/gnuradio/wiki/Volk.

[18] A. Ramos, "GNSS–SDR branch," Webpage, accessed 1 Set 2017, Source code downloadable from https://github.com/antonioramosdet/gnss-sdr.